

# Fabricating micro-structured surface by using single-crystalline diamond endmill

Jiawang Yan · Zhiyu Zhang · Tsunemoto Kuriyagawa · Hidenobu Gonda

Received: 10 February 2010 / Accepted: 20 April 2010 / Published online: 5 May 2010  
© Springer-Verlag London Limited 2010

**Abstract** A ball endmill made of single-crystalline diamond was used for cutting micro-structures on two kinds of mold materials, oxygen-free copper, and reaction-bonded silicon carbide (RB-SiC). The cutting performance of the ball endmill was investigated by examining surface roughness and form accuracy of the machined workpiece as well as tool wear characteristics. Micro-dimple arrays, micro-grooves, and micro-pyramid arrays with extremely smooth surface and high-accuracy profile could be obtained on oxygen-free copper without remarkable tool wear. When machining RB-SiC, however, tool flank wear takes place, leading to a rough surface finish. After the tool has worn off, the cutting performance of the endmill significantly depended on the tool feed direction. The optimum tool feed direction for micro-grooving was experimentally investigated.

**Keywords** Lens array · Dimple · Groove · Structured surface · End milling · Micro-cutting · Diamond tool · Tool wear · Mold fabrication · Hard material

## 1 Introduction

Structured surfaces, alternatively termed textured surfaces or engineered surfaces, are becoming more and more

important in advanced industrial technologies [1]. The ability to deterministically alter the topographic structure of a surface can have a profound effect on how that surface functions. The mechanical, optical, tribological, and fluidic characteristics, as well as many other properties, can be altered by fabricating textures and micro-structures on a flat or curved surface. Typical surface structures are micro-dimples arrays, prism arrays, pyramid arrays, and micro-grooves.

For example, a micro-lens array is a series of miniaturized lenses that formed in a one-dimensional or two-dimensional array on a supporting substrate. The ability of micro-lens arrays to focus incident light into a series of beam spots makes them useful in various applications, such as optoelectronic devices for optical communications and parallel image processing [2]. Micro-lens arrays on semiconductor substrates can be manufactured by silicon-based micro-machining methods, such as photolithography and etching technology [3, 4]. Recently, fabricating micro-lens arrays on plastics and glass has become a new research focus. As effective fabrication methods for plastic and glass components, plastic injection molding and glass molding press have received intensive attentions. In these replication processes, the fabrication of precision molding dies is important. It is difficult for photolithography and etching technology to fabricate micro-lens arrays on non-semiconductor mold materials with optical-quality surface finish and high-accuracy curved profiles.

An alternative approach is micro-endmilling. It has become popular to fabricate small structures with complicated shapes on various kinds of workpiece materials by endmilling. Endmilling is especially useful for machining high-precision and high-aspect ratio curved surfaces. For example, Weulel et al. [5] investigated micro-endmilling of tool steel with tungsten carbide (WC) tools for fabricating

---

J. Yan (✉) · Z. Zhang · T. Kuriyagawa  
Department of Nanomechanics, Tohoku University,  
Aramaki Aoba 6-6-01, Aoba-ku,  
Sendai 980-8579, Japan  
e-mail: yanjw@pm.mech.tohoku.ac.jp

H. Gonda  
Design Center, OSG Corporation,  
149 Miyamae, Ichinomiya-cho,  
Toyokawa, Aichi 441-1231, Japan

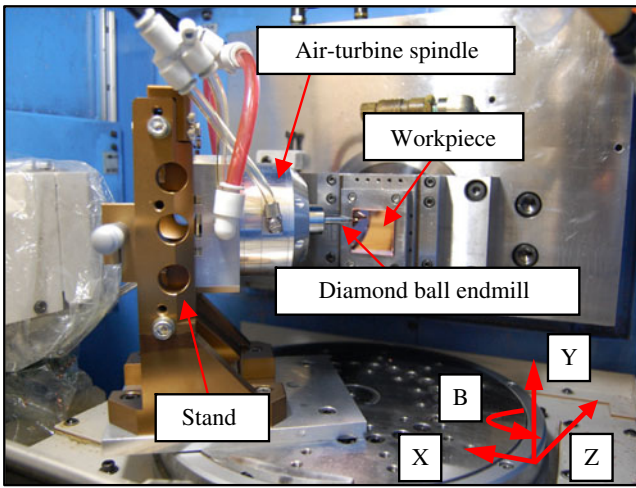


Fig. 1 Photograph of the experimental setup

molding dies. Kim and Kang [6] reported the high-speed endmilling of aluminum alloy using a specially designed poly-crystalline diamond endmill. Torres et al. [7] analyzed the performance of nano-crystalline diamond-coated micro-endmill in the machining of aluminum. However, to date, there are few reports on micro-endmilling with single-crystalline diamond tools. To obtain nanometer level surface finish and submicron level form accuracy, single-crystalline diamond tools are indispensable.

In the present work, an ultraprecision ball endmill was made using single-crystalline diamond as the tool material. The endmill was used to fabricate micro-structured molding dies. As a preliminary work, the cutting performance of this endmill in fabricating micro-dimple arrays and micro-grooves on two types of materials, namely, metal and ceramics, was experimentally investigated.

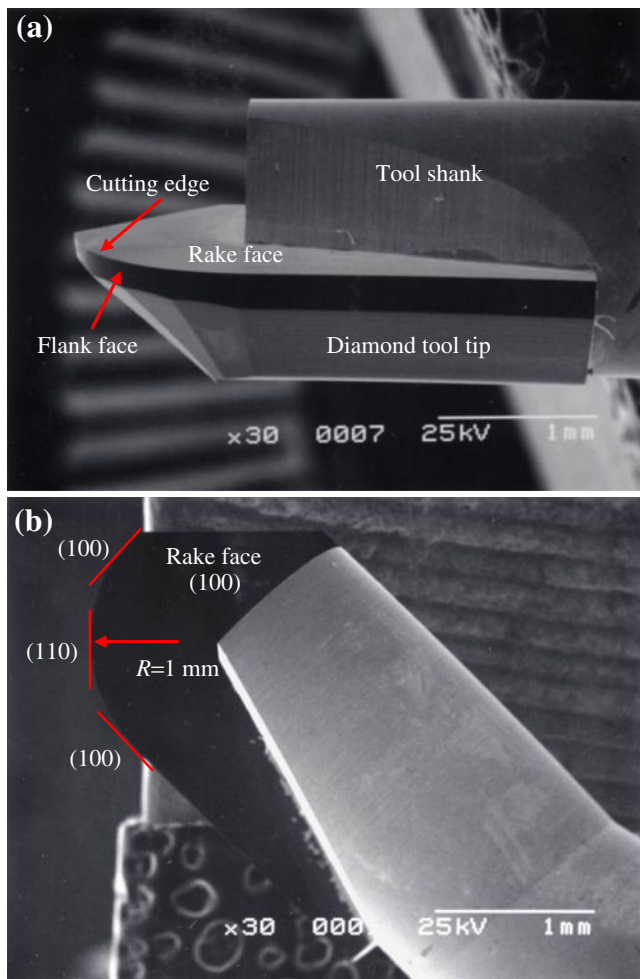


Fig. 2 SEM micrographs of the diamond ball endmill: a side view and b top view

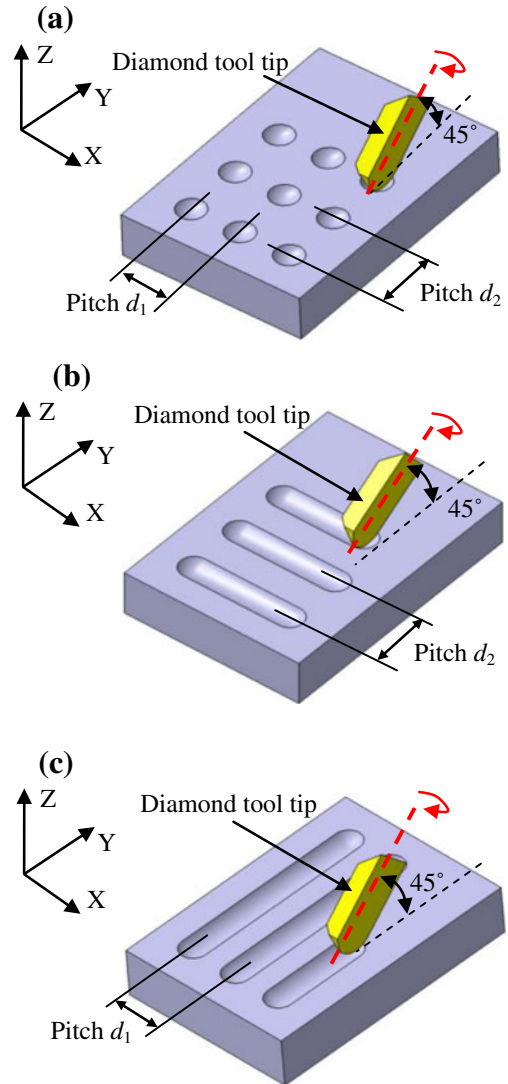
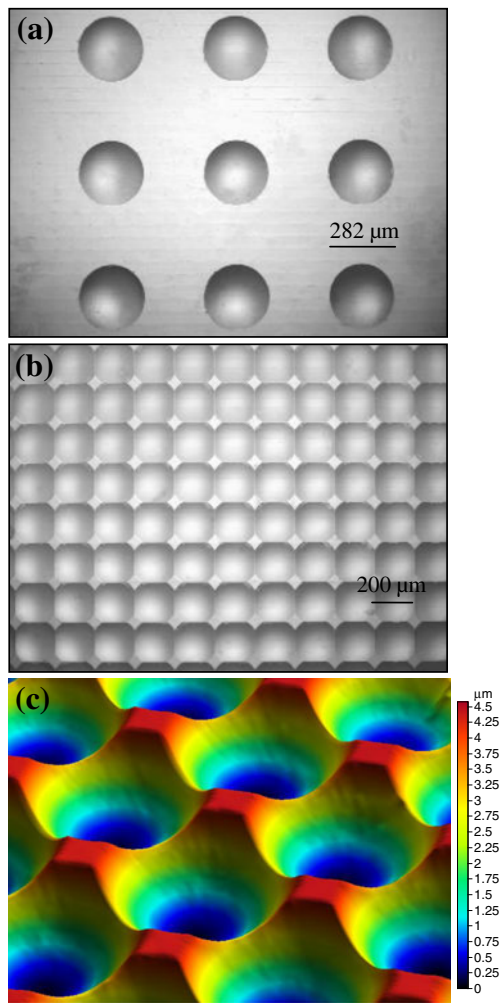


Fig. 3 Schematic models for a dimple array machining; b grooving method I; c grooving method II



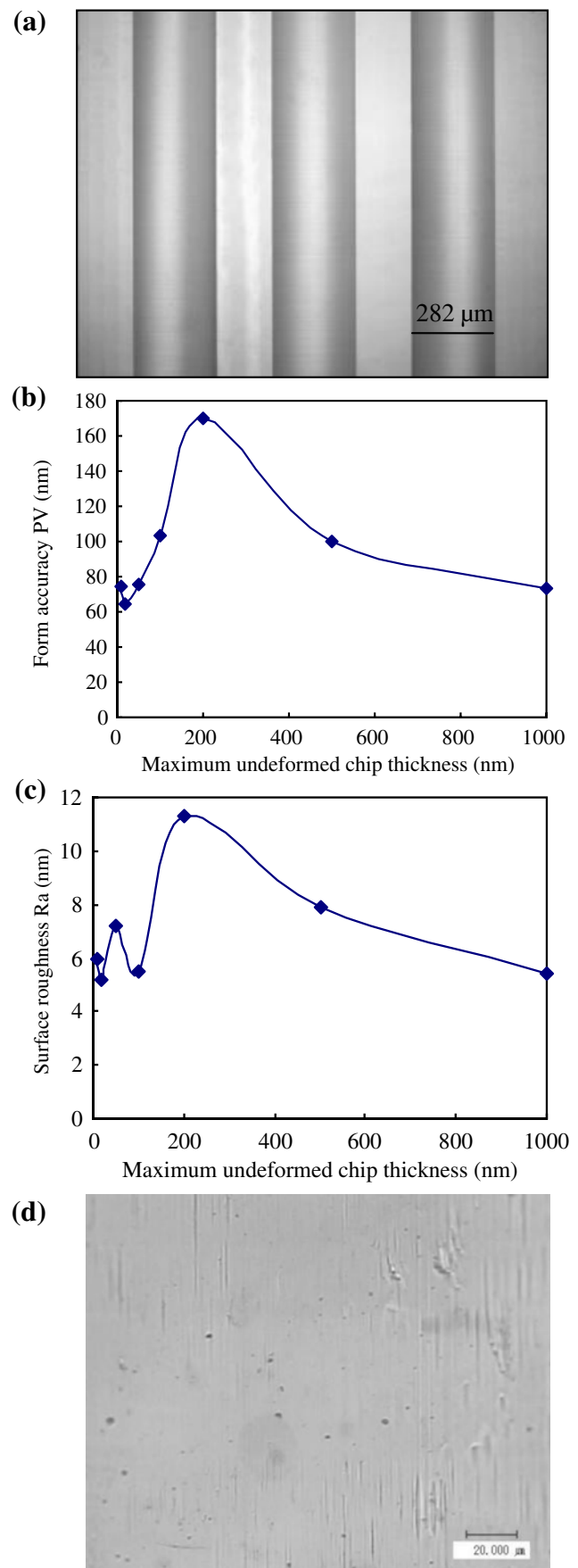
**Fig. 4** Micro-dimple arrays machined on copper: **a** optical image of separate dimples, **b** optical image of intersected dimples, and **c** three-dimensional topography of (c)

## 2 Experimental procedures

The micro-endmilling experiments were carried out on a four-axis (*XYZB*) numerical controlled ultraprecision machine tool, Toyoda AHN-05. The photograph of the main section of the machine is shown in Fig. 1. The resolution of the *X*-, *Y*-, and *Z*-axes tables is 1 nm and that of the *B*-axis is 1/10,000°. A high-speed precision air-turbine spindle is equipped in a stand mounted on the *B*-axis table.

A specially developed ball endmill, having a single-crystalline diamond tip bonded at the end of the shank, is gripped by a high-precision chucking mechanism in the spindle. Figure 2 shows scanning electron microscope

**Fig. 5** Micro-grooves machined on copper: **a** optical image of micro-grooves, **b** change of form error with  $t_{max}$ , **c** change of surface roughness with  $t_{max}$ , and **d** micrograph of the surface at  $t_{max}=200$  nm



(SEM) micrographs of the diamond endmill. The diamond tip is a round-nosed one with a designed radius of 1 mm, a  $0^\circ$  rake angle, and a  $10^\circ$  relief angle. The crystalline orientation of the tool rake face was (100) and that of the flank face was varied from (100) to (110) and then to (100) again along the  $90^\circ$  arc-shaped edge, as indicated in Fig. 2b.

Two kinds of workpieces were used in the experiments. One was oxygen-free copper (chemical composition, 99.99% Cu), which has a low hardness (1.6 GPa) and good machinability. Oxygen-free copper is a popular material for ultraprecision optical mirrors, as well as molding dies used in hot embossing of plastics and metallic glass [8]. The other workpiece material we used was reaction-bonded SiC (RB-SiC), provided by Japan Fine Ceramics Co., Ltd., which is composed of 6H-SiC grains (grain size  $\sim 1 \mu\text{m}$ , 88% in volume) and bonding silicon (12% in volume). RB-SiC is a promising material for fabricating molding dies used in glass molding press, but its ultraprecision machinability is very poor due to its high hardness (26.3 GPa) [9] and possible affinity of RB-SiC against diamond.

The workpiece was fixed on a stage which had been mounted onto the end of the main spindle box, namely, the Z-axis table. Before endmilling, a facing cut was performed for the oxygen-free copper workpiece using another diamond tool for providing a mirror-like surface. No pre-cut was performed for the RB-SiC workpiece because it was

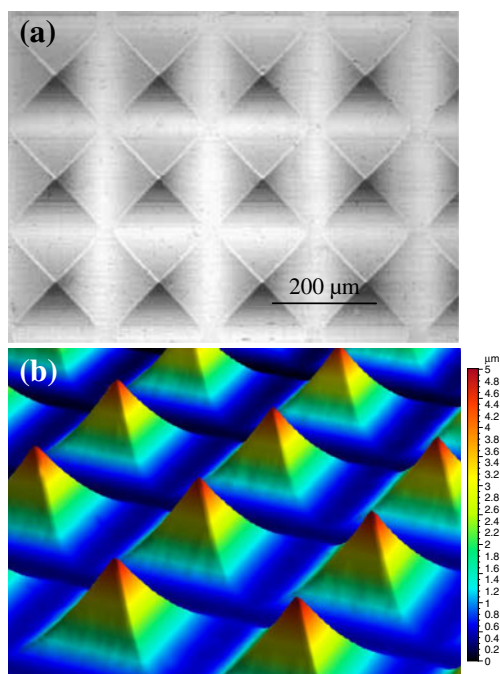


**Fig. 6** Micro-pyramids obtained by cross-grooving: **a** optical image, **b** three-dimensional topography

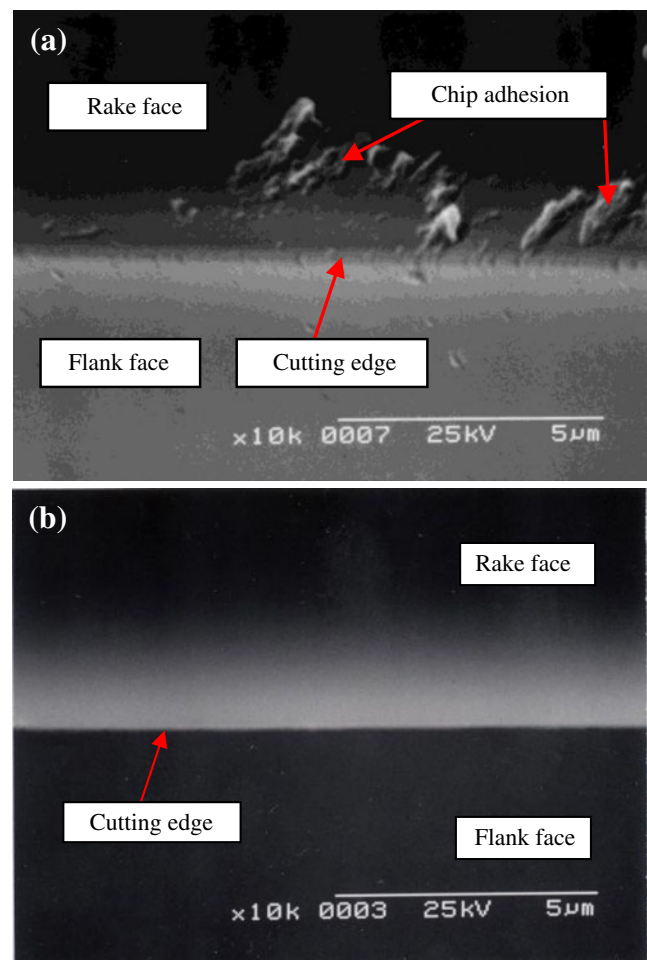


**Fig. 7** SEM micrographs of the cutting edge of a diamond ball endmill: **a** after machining 1,282 dimples and 200 mm-long grooves on oxygen-free copper; **b** the new edge before cutting experiments

provided with a polished mirror-like finish. The surface inclination of the workpiece with respect to the  $XY$  plane was carefully adjusted to less than  $1 \mu\text{m}$ . The endmill was inclined to an angle of  $45^\circ$  with respect to the workpiece surface by rotating the  $B$ -axis table. The rotation speed of the endmill was set to 20,000 rpm, and thus the maximum cutting speed was 1.48 m/s.

In this paper, three kinds of endmilling operations, as schematically shown in Fig. 3, were performed.

### 1. Dimple array machining

As shown in Fig. 3a, the endmill moves in the  $-Z$  direction, namely, the direction of depth of cut, to generate a single dimple, and then shifted by pitches  $d_1$  in  $X$  direction and  $d_2$  in  $Y$  direction to machine the other dimples. As a result, a two-dimensional micro-dimple array is fabricated. By changing the pitches, the dimples can be completely separated, partially intersected or fully intersected with each other.

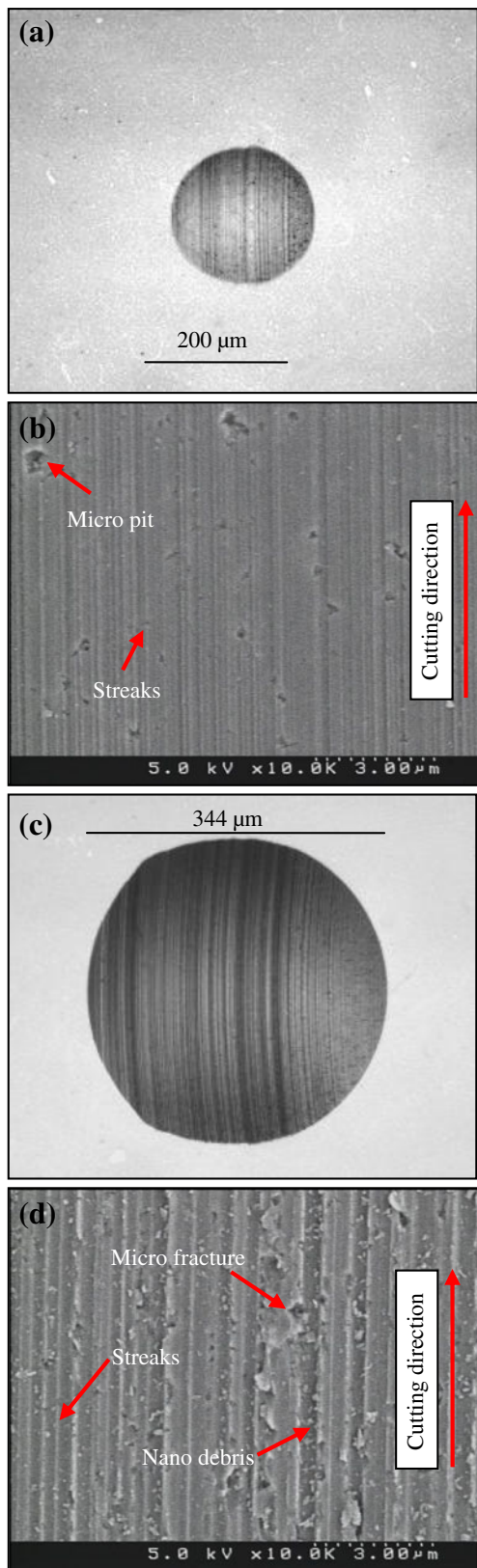


**Fig. 8** **a** Optical image and **b** SEM micrograph of the 1st micro-dimple machined on RB-SiC; **c** optical image; and **d** SEM micrograph of the 54th dimple

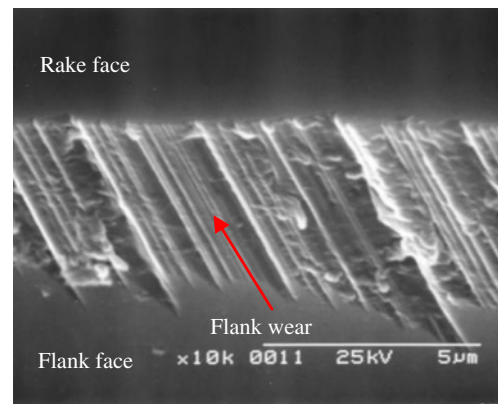


**Fig. 9** SEM micrograph of tool edge after machining 54 micro-dimples on RB-SiC

## 2. Grooving method I

As shown in Fig. 3b, the ball endmill feeds in  $X$  direction while keeping the depth of cut constant, to generate a single groove. Then, the endmill is shifted in  $Y$  direction to machine other grooves at a pitch of  $d_2$ . In this method, the tool feed direction is parallel to the cutting direction.

## 3. Grooving method II

As shown in Fig. 3c, the ball endmill feeds in  $Y$  direction to generate a groove, and then the endmill shifts in  $X$  direction by a pitch  $d_1$  to machine other grooves. In this method, the tool feed direction is perpendicular to the cutting direction.

## 3 Results and discussion

### 3.1 Machining of oxygen-free copper

In the experiments, firstly, oxygen-free copper was machined. Figure 4a shows a micrograph of a  $3 \times 3$  micro-dimple array. All the dimples have a diameter of  $282 \mu\text{m}$  and a depth of  $10 \mu\text{m}$ , and the pitch between two neighboring dimples is  $500 \mu\text{m}$ . All of the dimples are very smooth with a surface roughness of  $6 \text{ nm Ra}$ , and their profiles are very clear with a form error of  $67 \text{ nm}$ . Figure 4b shows a part of another micro-dimple array. The shape parameters of each dimple are the same as those in Fig. 4a while the pitches of the neighboring dimples are smaller ( $200 \mu\text{m}$ ). The dimples are partially intersected with each other, leaving rhombic flat regions among them. Figure 4c shows a three-dimensional topographical image of the micro-dimples in Fig. 4b. The surface topography was measured by a non-contact surface profilometer Mitaka NH-3SP with surface analysis software Mitaka Map. It can

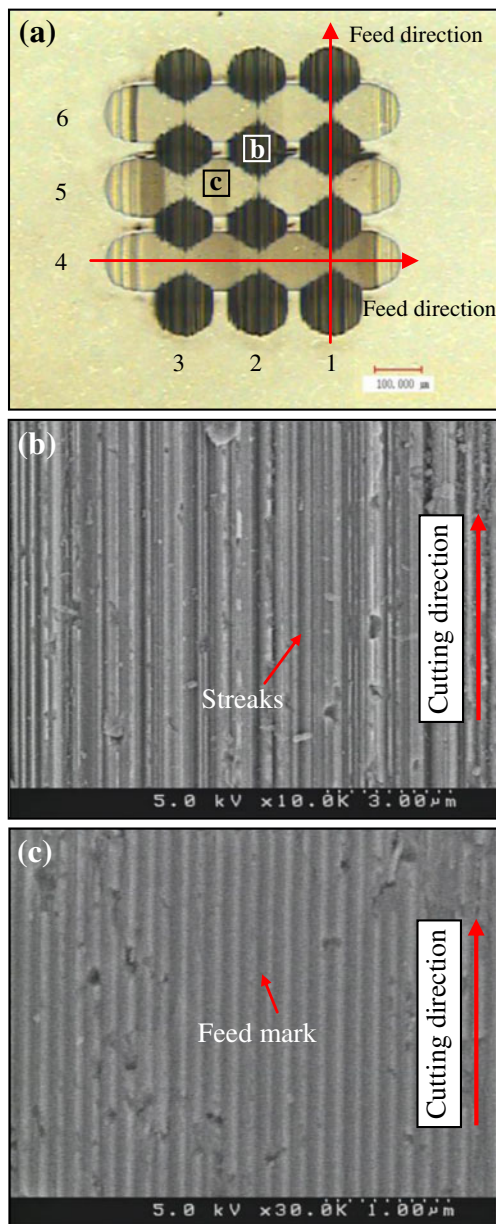


**Fig. 10** Micro-grooves machined on RB-SiC: **a** optical image of the crossing grooves; **b** and **c** are SEM micrographs of grooves 2 and 5, as indicated by **b** and **c** in **(a)**, respectively

be seen that the boundaries of the dimples are very sharp without burr formation.

Next, micro-grooves were machined by the grooving method I. The depth of cut was set to 10  $\mu\text{m}$ , and the tool feed was changed from 1.4 to 140 mm/min. As a result, the maximum undeformed thickness ( $t_{\text{max}}$ ) in one revolution of tool changes from 10 to 1,000 nm. Figure 5a shows a micrograph of three micro-grooves machined at  $t_{\text{max}}=100$  nm. The groove surfaces are very smooth with a roughness of 6 nm Ra. Figure 5b shows the change of form error, namely, PV of the cross-sectional profile error of the groove, with  $t_{\text{max}}$ . The profile was also measured by the

non-contact surface profilometer Mitaka NH-3SP. In the figure, the largest form error takes place at  $t_{\text{max}}=200$  nm. At a larger  $t_{\text{max}}$  ( $\sim 1,000$  nm), the form error is below 80 nm. Figure 5c shows the change in surface roughness with  $t_{\text{max}}$ . The largest surface roughness took place at  $t_{\text{max}}=200$  nm. Except this condition, an average surface roughness of 6 nm Ra could be obtained.

To make clear the cutting phenomenon at  $t_{\text{max}}=200$  nm, the groove surface was observed in detail. Figure 5d is a high-magnification micrograph of the groove surface. Numerous micro-scratches can be found on the surface, which indicates that built-up edges, namely, material stagnation ahead of the tool, might have occurred under this condition. Therefore, the selection of the tool feeding speed is important when machining copper, although it has good machinability.

Next, cross-grooving tests were performed by using both methods I and II. Figure 6a, b show a micrograph and a three-dimensional topography of the cross grooves machined at  $t_{\text{max}}=1,000$  nm, respectively. By cross-grooving, micro-pyramids are formed on the surface, the

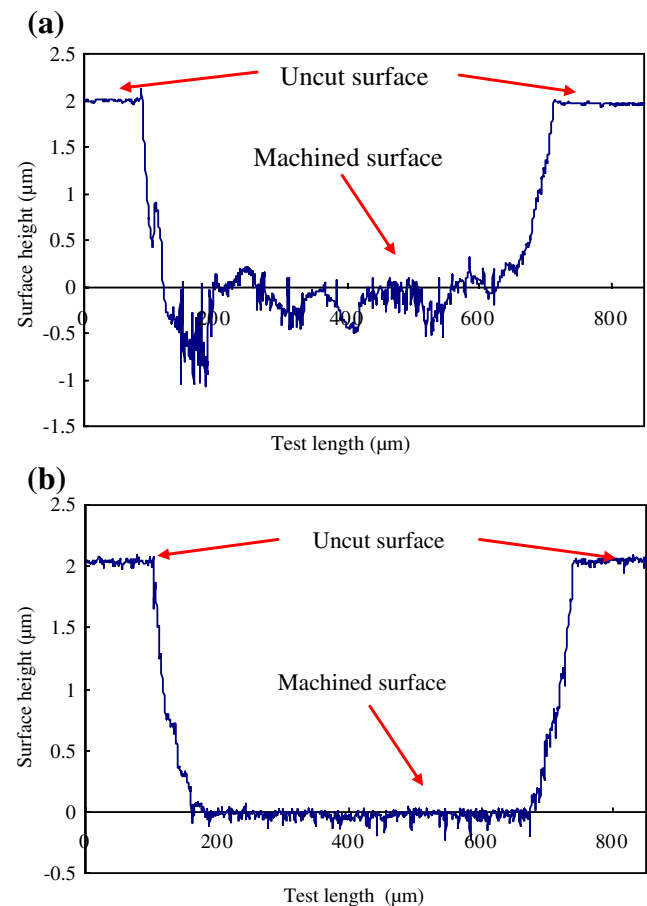


**Fig. 11** Longitudinal cross-sectional profiles of **a** groove 1 and **b** groove 4, measured along the tool feed directions as indicated in Fig. 10a

height and the pitch of which are 5 and 200  $\mu\text{m}$ , respectively. Burr formation and the material stagnation were not found under this condition.

After machining 1,282 dimples and 200 mm-long micro-grooves on copper, the endmill was observed under SEM to examine possible tool wear. Figure 7a shows an SEM micrograph of the used cutting edge. For comparison, the micrograph of the new cutting edge before experiments was shown in Fig. 7b. It can be seen that, after use, the cutting edge has been slightly rounded (Fig. 7a). However, the cutting edge is free of noticeable crater wear and flank wear. Therefore, we can conclude that when machining oxygen-free copper with a single-crystalline diamond ball endmill, the wear of diamond tool was insignificant.

### 3.2 Machining of RB-SiC

After the machining of the oxygen-free copper workpiece, endmilling experiments were conducted on the RB-SiC workpiece using the same diamond tool. Two kinds of dimple arrays were machined: separated dimples and intersected  $3 \times 3$  dimple arrays. For each kind of dimple, the total depth of cut was set to 5, 10, and 15  $\mu\text{m}$ , respectively. As a result, a total of 54 micro-dimples were machined on the RB-SiC workpiece.

Figure 8a, b show an optical image and an SEM micrograph of the first micro-dimple machined on RB-SiC, which has a diameter of 200  $\mu\text{m}$  and a depth of 5  $\mu\text{m}$ . As seen in Fig. 8a, the dimple is nearly round (form error:

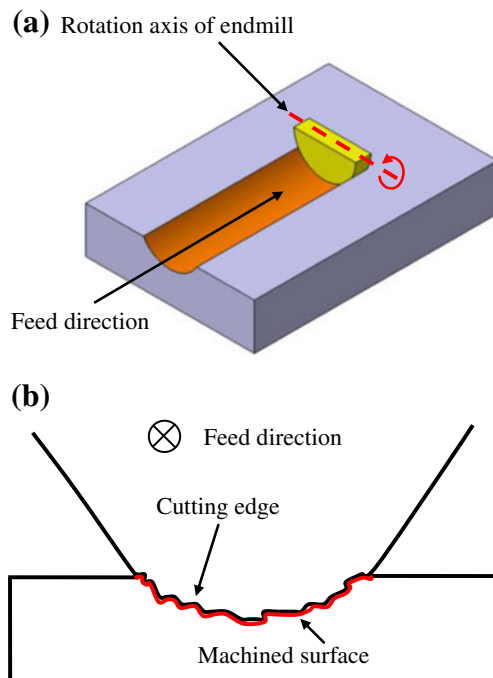


**Fig. 12** Surface generation models for grooving method I: **a** three-dimensional model and **b** two-dimensional model

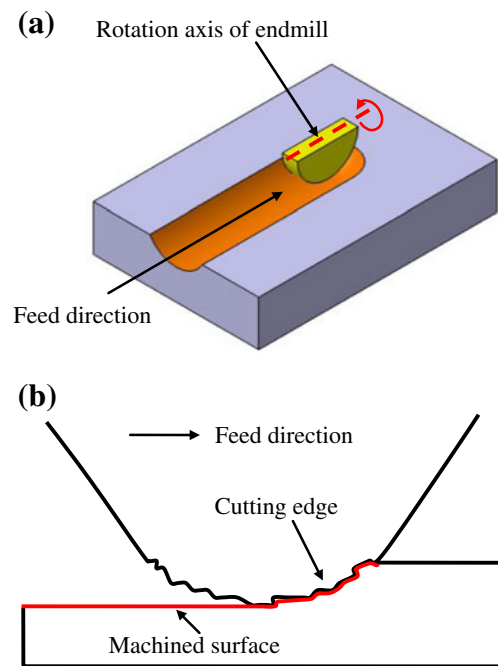


**Fig. 13** Surface generation models for grooving method II: **a** three-dimensional model and **b** two-dimensional model

211 nm), and the surface is basically smooth (surface roughness, 17 nm Ra). Figure 8b is a magnified view of the dimple surface, where we can see that the surface is machined in a ductile mode. A few submicron-sized micro-pits can be observed on the surface, which are presumably caused by dislodgement of SiC grains from the machined surface, similar to those observed in diamond turning experiments [9]. In addition, a few nano-level streaks oriented along the cutting direction are observed on the surface.

Figure 8c, d shows an optical image and an SEM micrograph of the 54th micro-dimple, which has a diameter of 344  $\mu\text{m}$  and a depth of 15  $\mu\text{m}$ . In Fig. 8c, a few deep streaks can be seen on the dimple surface. Figure 8d is a magnified view of the dimple surface. Although a ductile-machined surface appearance can be identified, deep streaks, micro-pits, and small debris make the surface very rough.

After machining 54 micro-dimples on the RB-SiC workpiece, the endmill was observed again under SEM to examine tool wear. Figure 9 shows an SEM micrograph of the cutting edge. A wide wear land is seen at the flank face of the endmill. The wear land is very rough, with many scratches and grooves. These results demonstrate that when endmilling RB-SiC, although ductile mode material removal can be realized, the diamond ball endmill will wear significantly in the later stage, leading to deep streaks on the machined surface.

Finally, micro-grooving tests were performed on the RB-SiC workpiece using the worn tool shown in Fig. 9. Two kinds of grooving tests, method I and II, as shown in

Fig. 3b, c, were performed respectively, by changing the tool feed direction with respect to the cutting direction.

Figure 10a shows an optical image of six crossing micro-grooves machined on the RB-SiC sample. Grooves 1, 2, and 3 were machined by the grooving method I (Fig. 3b), and grooves 4, 5, and 6 were obtained by the grooving method II. The tool feed rate when machining all the grooves was 3 mm/min. The two kinds of grooves showed distinct differences: the surfaces of grooves 1, 2, and 3 are very rough while those of grooves 4, 5, and 6 are very smooth. Figure 10b, c are magnified SEM micrographs of groove 2 (indicated by b in Fig. 10a) and groove 5 (indicated by c in Fig. 10a), respectively. Deep streaks are observed in Fig. 10b. In contrast, very shallow periodical tool feed marks are seen on the surface, indicating a stable ductile-machining mode.

Figure 11a, b show cross-sectional profiles of grooves 1 and 4, respectively, measured longitudinally along the tool feed directions as indicated by red arrows in Fig. 10a. The flatness of the groove bottoms is distinctly different. The surface roughness of groove 1 is 86 nm Ra and 853 nm Rz, while that of the groove 4 is 26 nm Ra and 200 nm Rz.

Three- and two-dimensional surface generation models for grooving method I are shown in Fig. 12a, b, respectively. As the tool feed direction is perpendicular to the endmilling rotational axis, after the cutting edge has worn, the unevenness on the flank wear land of the tool will be replicated onto the machined surface, forming deep parallel streaks. In grooving method II, however, the tool feed direction is parallel to the endmill rotational axis, as shown in Fig. 13a. Therefore, the finished surface is generated by the same point on the cutting edge, namely, the lowest point in Fig. 13b. In this case, even if the cutting edge has worn, a smooth surface might be obtained. From this point of view, we can conclude that the grooving method II is preferable to the grooving method I in micro-endmilling of hard materials.

#### 4 Conclusions

A single-crystalline diamond ball endmill has been used for generating micro-surface structures on two kinds of mold materials, oxygen-free copper and RB-SiC, respectively, and the cutting performance of the endmill was investigated experimentally. The following conclusions were obtained:

1. Precise micro-structures, such as micro-dimple arrays, micro-grooves, and micro-pyramid arrays, can be

obtained on oxygen-free copper with an average surface roughness of 6 nm Ra. Slight edge rounding occurs to the endmill, while rake wear and flank wear of the tool are insignificant.

2. Undeformed chip thickness (determined by tool feed rate) is an important factor affecting the surface quality when machining oxygen-free copper. Under the present experimental conditions, an undeformed chip thickness of 200 nm should be avoided.
3. When endmilling RB-SiC, ductile mode material removal can be realized, while the endmill wears significantly in the later stage, leading to deep streaks on the machined surface.
4. In micro-grooving of RB-SiC, selection of tool feed direction is important. By feeding the endmill along the same direction as the tool rotational axis, a smooth surface can be obtained even after the cutting edge has worn.

**Acknowledgements** We would like to extend our thanks to Japan Fine Ceramics Co., Ltd., for providing the RB-SiC samples and OSG Corporation for providing help in developing the single-crystalline diamond tools for the experiments in this study.

#### References

1. Evans C, Bryan J (1999) “Structured” “textured” or “engineered” surfaces. *CIRP Ann* 48:541–556
2. Lim C, Hong M, Lin Y, Chen G, Kumar A, Rahman M, Tan L, Fuh J, Lim G (2007) Sub-micron surface patterning by laser irradiation through microlens arrays. *J Mater Process Technol* 192–193:328–333
3. Däschner W, Long P, Stein R, Wu C, Lee S (1996) General aspheric refractive micro-optics fabricated by optical lithography using a high energy beam sensitive glass gray-level mask. *J Vac Sci Technol B* 14:3730–3733
4. Totsu K, Fujishiro K, Tanaka S, Esashi M (2006) Fabrication of three-dimensional microstructure using maskless gray-scale lithography. *Sensor Actuator A* 130–131:387–392
5. Weule H, Hüntrup V, Tritschler H (2001) Micro-cutting of steel to meet new requirements in miniaturization. *CIRP Ann* 50:61–64
6. Kim J, Kang Y (1997) High-speed machining of aluminium using diamond endmills. *Int J Mach Tools Manuf* 37:1155–1165
7. Torres C, Heaney P, Sumant A, Hamilton M, Carpick R, Pfefferkorn F (2009) Analyzing the performance of diamond-coated micro end mills. *Int J Mach Tools Manuf* 49:599–612
8. Pan C, Wu T, Liu Y, Yamagata Y, Huang J (2009) Fabrication of aspheric surface using ultraprecision cutting and BMG molding. *J Mater Process Technol* 209:5014–5023
9. Yan J, Zhang Z, Kuriyagawa T (2009) Mechanism for material removal in diamond turning of reaction-bonded silicon carbide. *Int J Mach Tools Manuf* 49:366–374